Contract No:

This document was prepared in conjunction with work accomplished under Contract No. 89303321CEM000080 with the U.S. Department of Energy (DOE) Office of Environmental Management (EM).

Disclaimer:

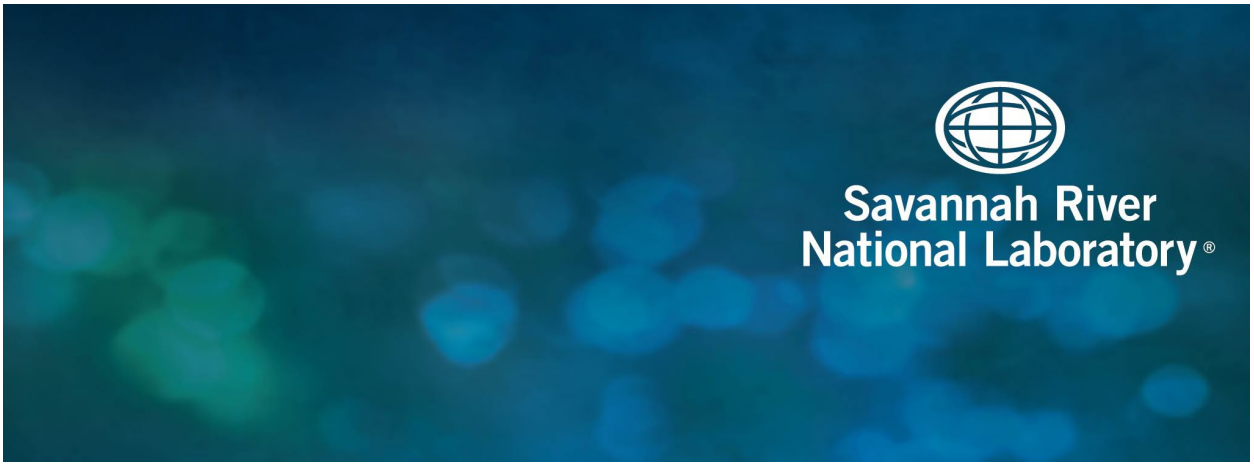

A U.S. DEPARTMENT OF ENERGY NATIONAL LAB • SAVANNAH RIVER SITE • AIKEN, SC • USA

Review and Summary of Oxide Thickness Data for Aluminum-Clad Spent Nuclear Fuel

Anna. L. d'Entremont

Robert L. Sindelar

February 14, 2023

SRNL-STI-2023-00038, Revision 0

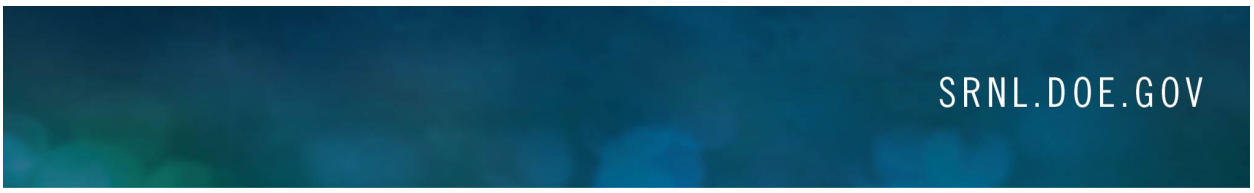

DISCLAIMER

Printed in the United States of America

Prepared for
U.S. Department of Energy

SRNL-STI-2023-00038
Revision 0

Keywords: *aluminum (oxy)hydroxide, bayerite, gibbsite, boehmite*

Retention: *Varies*

Review and Summary of Oxide Thickness Data for Aluminum-Clad Spent Nuclear Fuel

Anna. L. d'Entremont
Robert L. Sindelar

February 14, 2023

Savannah River National Laboratory is operated by Battelle Savannah River Alliance for the U.S. Department of Energy under Contract No. 89303321CEM000080.

REVIEWS AND APPROVALS

AUTHORS:

_____
Anna. L. d'Entremont, Savannah River National Laboratory Date

_____
Robert L. Sindelar, Savannah River National Laboratory Date

TECHNICAL REVIEW:

_____
Bruce Wiersma, Savannah River National Laboratory, Reviewed per E7 2.60 Date

APPROVAL:

_____
Boyd Wiedenman, Manager Date
Separation Sciences and Engineering, Savannah River National Laboratory

_____
Frank Pennebaker, Manager Date
Chemical Processing and Characterization Division, Savannah River National Laboratory

_____
Elmar F. Eidelpes, Idaho National Laboratory Date

PREFACE

Hydrated oxides form on aluminum-clad nuclear fuel under service conditions of reactor irradiation and post-discharge water storage. A review of the literature is performed to compile the understanding of the mechanisms of film formation, the models for film growth, and the available data from post-irradiation characterizations of fuel materials. The results will be used to provide input into engineering analyses to support the drying and sealed dry storage of aluminum-clad spent nuclear fuel.

EXECUTIVE SUMMARY

The U.S. Department of Energy (DOE) owns a large inventory of aluminum-clad spent nuclear fuel (ASNF) in interim storage pending ultimate disposition, with more being generated by currently operating research reactors. Dry storage in sealed DOE Standard Canisters is being investigated as an approach for long-term interim storage and/or disposition in a repository for ASNF.

A primary challenge for ASNF storage is the presence of aluminum (oxy)hydroxide layers formed on the cladding surfaces during water exposure in the reactor and in wet storage, which forms a reservoir of chemisorbed water not readily removed at low (<100°C) drying temperatures. Free, physisorbed, and chemisorbed water are all susceptible to radiolytic breakdown under irradiation and can release hydrogen gas. Identifying the likely range of (oxy)hydroxide loadings on ASNF that may be placed in dry storage will help to ensure that the impact of the (oxy)hydroxide is adequately accounted for while avoiding over-conservatism and enable mitigation strategies to be implemented where needed.

The current report summarizes information on (oxy)hydroxide thicknesses and characteristics from the literature and from recent measurements taken in the present research campaign. In general, corrosion studies have indicated that the corrosion and oxide buildup on aluminum are affected by numerous conditions, including pH, temperature and heat flux, coolant flowrates, irradiation (in-reactor vs. unirradiated tests), duration of water exposure, and the amount of oxide already on the surface. Some of these factors are interrelated (e.g., the local temperature, heat flux, and coolant flowrate). Observations of the impact of irradiation (in-reactor versus ex-reactor measurements) on corrosion and oxide thickness are mixed, but multiple studies indicate that there is a significant difference between in-reactor and ex-reactor corrosion kinetics, even when other operating conditions such as pH, flowrate, heat flux, etc., simulate those in a reactor.

Systematic oxide thickness data on actual ASNF available in the literature is limited. Available data indicates that localized oxide thicknesses can reach relatively high values, up to a maximum of 80 μm for one study. A subset of the studies reviewed reported systematic oxide thickness measurements spaced across the surface of a fuel element, and the averages of these sets of systematic measurements fell in the range 12–25 μm. Oxide thicknesses tended to be highest in the central portion of the plate, with lower thicknesses near the ends.

This literature survey indicates that average oxide thicknesses of 12–25 μm are reasonable for ASNF plates, including on elements from the Advanced Test Reactor and High Flux Isotope Reactor. The localized maximums may be several times higher, and, due to the oxide distributions, measurements taken close to the edges of the fuel may underestimate the oxide loading. Unfortunately, the spread of available data and the variety of prefilm, reactor service, and post-discharge storage conditions does not enable identification of a bounding oxide thickness, and average oxide thicknesses exceeding 25 μm for ASNF may occur.

TABLE OF CONTENTS

LIST OF TABLES

LIST OF FIGURES

LIST OF ABBREVIATIONS

ASNF	Aluminum-clad spent nuclear fuel
ATR	Advanced Test Reactor
DOE	U.S. Department of Energy
DSC	DOE Standard Canister
HFIR	High Flux Isotope Reactor
MURR	Missouri University Research Reactor
RERTR	Reduced Enrichment for Research and Test Reactors Program
SEM	Scanning electron microscopy
SNF	Spent nuclear fuel
SRS	Savannah River Site
TGA	Thermogravimetric analysis
XRD	X-ray diffraction

1.0 Introduction

The U.S. Department of Energy (DOE) owns a large inventory of aluminum-clad spent nuclear fuel (ASNF) in interim storage pending ultimate disposition, with more being generated by currently operating research reactors. The current disposition path for DOE-owned ASNF is chemical dissolution and processing, for which only one facility exists in the USA. Dry storage in sealed canisters is an established long-term storage approach for commercial (Zr-clad) spent nuclear fuel (SNF) and is a potential alternative pathway for interim storage and/or disposition of ASNF. Interim storage pending disposition in an SNF repository must be prepared for an extended storage duration (>50 years) since no repository location currently exists. The current report is part of a research program [1] to support a technical basis for extended dry storage of ASNF in DOE Standard Canisters (DSCs).

The water content associated with spent nuclear fuel must be considered for drying and placement in a sealed dry storage canister to ensure the residual water (post-drying) does not exceed the design criteria of the canister [2]. A core challenge for ASNF storage is the existence of chemically bound water on the cladding surface in the form of aluminum (oxy)hydroxides, which form when aluminum cladding surfaces are exposed to water, e.g., in the reactor and in subsequent wet storage. This reservoir of chemisorbed water is not readily removed at low (<100°C) drying temperatures. Free, physisorbed, and chemisorbed water are all susceptible to radiolytic breakdown under irradiation and can release hydrogen gas. Therefore, the current project [1] has investigated characteristics, drying behavior, and radiolytic H_2 yields associated with adherent aluminum (oxy)hydroxide films.

Identifying the likely range of (oxy)hydroxide loadings on ASNF that may be placed in dry storage provides realistic inputs for safety assessments while avoiding over-conservatism. Potential approaches for addressing packaging of thick (oxy)hydroxide films could include measures such as high-temperature drying to partially decompose trihydroxides or adjusting the fuel load per canister to ensure that the total (oxy)hydroxide content is sufficiently low to ensure canister conditions would not exceed canister design under extended service. An accurate assessment of realistic oxide loading would enable use of these extra precautions only where needed.

No reliable model currently exists to assess (oxy)hydroxide growth on a fuel element over possible service time histories including from prefilming to irradiation to pool storage. Therefore, the literature information on aluminum oxide formation and growth is assembled for input for the DSC analyses. The focus is on service conditions for aluminum-clad fuel and a review of the available literature reporting the formed oxides, the thickness and type, as available.

The present report summarizes information on thicknesses and characteristics of adherent aluminum (oxy)hydroxide films on ASNF from the literature and from measurements taken in the current program. Limited information on literature (oxy)hydroxide growth models and hypothesized physical mechanisms is included for context.

2.0 Background

2.1 Aluminum oxide types and characteristics

Oxide types relevant to ASNF cladding include alumina (Al_2O_3), the aluminum oxyhydroxide boehmite (AlOOH or $Al_2O_3 \cdot H_2O$), and the aluminum trihydroxide polymorphs bayerite and gibbsite ($Al(OH)_3$ or $Al_2O_3 \cdot 3H_2O$). Other polymorphs of both $Al(OH)_3$ and AlOOH exist but are not commonly reported in studies of aluminum corrosion. These oxides do not always appear in isolation; multi-layered and mixed adherent oxide films are reported in various studies. Boehmite-bayerite dual layers typically feature bayerite on the outer surface, with boehmite sandwiched between the bayerite and the metal [3].

Alumina makes up the thin passivation film that forms almost instantaneously on aluminum metal exposed to oxygen. The (oxy)hydroxides form under exposure to water, either directly from the reaction of aluminum metal with water or by reaction of an existing oxide (Al_2O_3 or AlOOH) with water to form a more-hydrated oxide (AlOOH or $Al(OH)_3$) [4]. All the reactions of aluminum metal with water result in the formation of 1.5 moles of H_2 per mole of aluminum metal reacted [4].

2.1.1 Boehmite and pseudoboehmite

Crystalline boehmite (AlOOH) is generally expected to form above 80°C [5] and is thermodynamically metastable [4]. It consists of a layered structure, as illustrated in Figure 2-1, with adjacent layers linked by hydrogen bonds between the hydroxl ions, and has a density of 3.01 g/cm^3 [4].

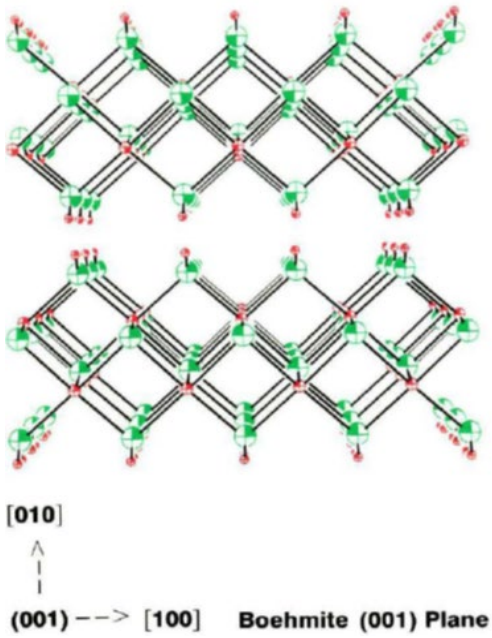

Figure 2-1. Crystal structure of boehmite [4]. The larger red-and-white spheres represent Al, green-and-white spheres O, and smaller red-and-white spheres H.

Another commonly reported phase for aqueous corrosion of aluminum is "pseudoboehmite," a poorly crystallized (oxy)hydroxide with an XRD pattern similar to that of boehmite but water content exceeding the ~15 wt.% for stoichiometric AlOOH, with reported values up to 30 wt.% water [4, 6]. Its XRD peaks are broader that those of well-crystallized boehmite due to lower crystallinity, and the distance between adjacent layers increases slightly (from ~6.15 Å in well-crystallized boehmite to as much as 6.6–6.7 Å) [6].

Various hypotheses have been proposed for what position the excess water occupies in pseudoboehmite, including existing as molecular water between "boehmite-like layers", occupying oxygen or hydroxyl sites in the chains, or adjacent particle surfaces being linked through hydrogen bonding with a layer of chemisorbed water [4, 6]. Baker and Pearson [6] suggest that the 0.7 Å increase in crystal spacing indicated by XRD is unlikely to accommodate much molecular water and note that even "dry" pseudoboehmite (indicated by nuclear magnetic resonance spectroscopy to have only chemisorbed and not physisorbed water) still exceeded the water content of stoichiometric boehmite. They instead proposed that pseudoboehmite is an aggregate of very small boehmite-like crystallites, with the excess water corresponding to surface hydration on the large specific surface area, which is consistent with experimental observations that the water content of pseudoboehmite increased with decreasing crystal size [6].

(Oxy)hydroxides identified as either boehmite or pseudoboehmite have been identified in several studies of (oxy)hydroxide growth in water at relatively low temperatures (40°C to 100°C) [5, 7, 8], and laboratory studies of the formation of aluminum (oxy)hydroxides have suggested that pseudoboehmite forms as a preliminary corrosion product that ages into more crystalline forms of either AlOOH or $Al(OH)_3$.

2.1.2 Aluminum trihydroxides: Bayerite and gibbsite

Aluminum trihydroxides ($Al(OH)_3$) come in several polymorphs, including bayerite and gibbsite [9]. Gibbsite appears in natural bauxites, while natural bayerite is rare [4], but bayerite is the more commonly observed trihydroxide polymorph for aqueous corrosion of aluminum metal [3].

All of the trihydroxide polymorphs have a layered structure that can be represented as sheets of $Al(OH)_6$ octahedra, forming hexagonal rings of Al [4, 9]. As in AlOOH, the layers are held together by interlayer hydrogen bonds, and polymorphs are distinguished by the stacking sequence of the layers and the O-H bond orientation [9]. In gibbsite, the hydroxyl groups of adjacent layers are directly opposite one another, leaving channels through the lattice perpendicular to the sheets [4] (Figure 2-2). Bayerite consists of the same sheet structure as gibbsite, with the hydroxyl groups of adjacent layers offset from one another [4]. Both polymorphs contain the same amount of water per mole, but differ slightly in density: 2.42 g/cm^3 for gibbsite and 2.53 g/cm^3 for bayerite [4].

Wefers and Misra [4] noted that the relative stability and driving forces behind the formation of the various trihydroxide polymorphs is subject to debate, but impurities appear to play an important role. Synthesis from "very pure" aluminum and water or from hydrolysis of pure, active alumina reportedly always results in bayerite, while aging in other solutions triggers transformations to other polymorphs, e.g., NH_3 solutions yield nordstrandite while NaOH or KOH solutions yield gibbsite [4].

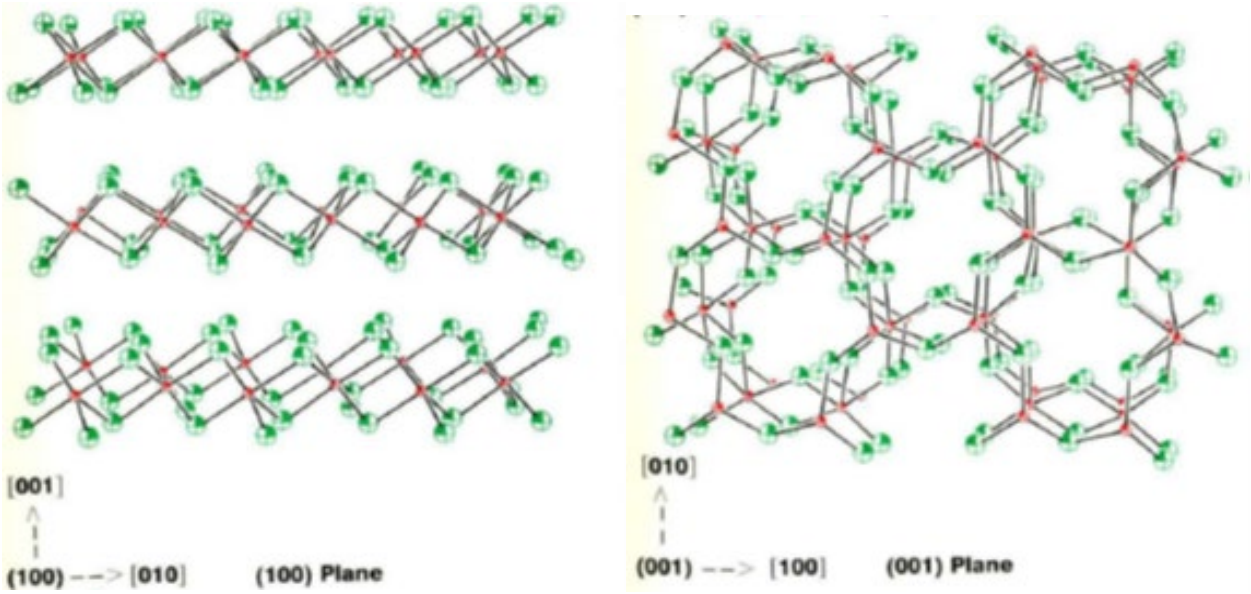

Figure 2-2. Crystal structure gibbsite, viewed along the plane of the layers (left) and facing the plane of the layers (right) [4]. The red spheres represent Al and the green-and-white spheres OH groups.

2.1.3 Aluminum oxide/alumina

Aluminum oxide or alumina (Al_2O_3) can be formed by direct oxidation of aluminum metal or by thermal/hydrothermal dehydration of aluminum (oxy)hydroxides [4]. A very thin (2–4 nm) protective Al_2O_3 layer forms on aluminum metal under oxygen or dry air at room temperature, which is generally considered

to be non-crystalline, although a short-range, cubic ordered structure has been observed in some studies [4]. Direct oxidation of aluminum metal forms crystalline alumina only at high temperature, above about 650 K (380°C) [4].

Corundum (α-Al_2O_3) is the only thermodynamically stable aluminum oxide, with a crystal structure consisting roughly of alternating layers of oxygen and aluminum ions [4].

2.2 ASNF corrosion conditions

Aluminum-clad fuel goes through multiple stages in its post-fabrication service. This service may involve prefilming and various water exposure, temperature, and duration during irradiation and wet storage. That is, as a material set, ASNF does not have a single standard oxide type and thickness condition.

2.2.1 Prefilming

Some aluminum-clad fuel is deliberately corroded prior to use in the reactor with the intent to form a protective oxide film that will slow further corrosion. Advanced Test Reactor fuel is a notable example, having a high-temperature prefilming process designed to produce a thin boehmite film. Details of prefilming processes will be described later as relevant to oxide thickness studies.

2.2.2 In-reactor

During reactor operation, the outer surface of the cladding is exposed to coolant, often flowing light or heavy water, which may include additives intended to control pH or inhibit corrosion as well as radiolysis products due to the ionizing radiation. Literature studies [3, 10] indicate that exposure to flowing water erodes aluminum oxide films, making them less protective against further corrosion. Multiple researchers [3, 10] have also hypothesized that different oxides dissolve selectively, which may result in porous oxides that are less protective than a dense film of the same nominal thickness. The solubility of aluminum (oxy)hydroxides is known to vary with pH, with a minimum in near-neutral solutions and increasing solubility in both acidic and basic solutions [4]. Shaber and Hofman [11] identify the center of the "passivation region" as pH of 5.4–6.0. The ATR and HFIR are controlled to a slightly lower pH of 5 based on results from an unirradiated test loop [12] indicating a minimum corrosion rate at that pH [11].

Heat generated by fission within the fuel causes significant heat flux across the cladding from the fuel to the coolant, and the temperature of the cladding depends on details of the reactor operation, including coolant inlet temperature, flowrate, the magnitude of the heat flux through the cladding, and the current local oxide thickness. The thermal conductivity of the aluminum (oxy)hydroxides is significantly lower than that of aluminum metal, so the presence of an oxide film can significantly raise the temperature of the fuel and result in a substantial temperature drop across the oxide film. Experiments in test loops designed to replicate reactor heat transfer and fluid flow characteristics have measured temperature drops reaching ≥120°C across the oxide, and this large temperature drop appears to be correlated with oxide spallation [13, 14]. Oxide thicknesses reached prior to spallation varied widely (17 to 50 μm) at different heat fluxes (20 to 5 MW/m^2), but generally did not occur until the temperature drop across the oxide exceeded 120°C [13, 14].

Cladding is also exposed to significant irradiation during oxide growth in the reactor and in post-reactor storage. The direct impact of neutron bombardment and the chemical effects of radiolysis products on the corrosion process and oxide film is not well established. Corrosion experiments on aluminum alloy samples (with no fuel meat) exposed in in-reactor and out-of-reactor sections of the same test loop [15] concluded that the in-reactor section was "less corrosive" than the out-of-reactor section when they compared the amount of aluminum metal lost after chemically stripping the oxide. By contrast, a model fitted to both in-reactor and out-of-reactor data from various sources [16] suggested that in-reactor conditions were "more favorable for oxide growth."

2.2.3 Wet (pool) storage

Wet storage pools are used to store ASNF both after discharge from a reactor or as temporary storage between different cycles in the reactor. In comparison to the reactor conditions, the average pool water is lower in temperature and nominally still. For example, conditions documented for the SRS L Basin wet storage pool conditions over a 26-year period had an average temperature near 22°C (range 14.6–28°C) and average pH of 6.5 [17]. Residual decay in a discharged fuel element will continue to generate radiation and heat flux through its cladding, with both the radiation dose rate and heat flux decreasing over time.

Oxide forming during this period will form on a surface with a pre-existing (oxy)hydroxide film from in-reactor exposure, altering the corrosion behavior compared to those of a fresh aluminum surface in the same environment. However, in some cases, components such as end boxes, etc., are cut off for storage, exposing a limited amount of fresh aluminum surface on a small fraction of the surface area.

3.0 Growth of (oxy)hydroxide films on aluminum

3.1 Characteristics of (oxy)hydroxide formation in water

Numerous lab studies of aluminum corrosion and (oxy)hydroxide formation have investigated characteristics of the reaction and the influence of various corrosion conditions. Numerous factors have been found to influence the corrosion and oxide layer growth, with both temperature and pH identified as major factors. Even small changes in the pH have been found to result in substantial changes to the oxide formation; testing in reactor-relevant pH ranges (often targeted around pH 5.0) found that increasing pH correlated with more rapid oxide growth [12, 18]. Similarly, correlations targeting reactor-relevant conditions generally predict faster oxide growth with increasing temperature [3, 12, 18].

Oxide dissolution into the water and precipitation back onto the surface as (oxy)hydroxide has been hypothesized as a key part of the aqueous corrosion process [7, 19]. The proposed mechanism is formation of an amorphous Al_2O_3 as the initial product of the aluminum and water reaction, dissolution of Al_2O_3 into the water, and finally precipitation of the dissolved species onto the surface as platelets of pseudoboehmite. A similar dissolution and re-precipitation process would allow pseudoboehmite to age into more crystalline forms such as bayerite, gibbsite, or boehmite (depending on environmental conditions) [7]. The need for an oxide dissolution process for oxide film formation could account for the much lower corrosion rates observed under exposure to moist air or to (liquid) solutions with low solubility for Al_2O_3 relative to those in liquid water [7].

Experimental studies of aluminum corrosion under simulated reactor conditions, such as Ref. [15], have observed formation (deposition) of aluminum (oxy)hydroxides on non-aluminum components in the cooling system, confirming that (oxy)hydroxide precipitation out of solution does occur. Similarly, the corrosion resistance of later samples was observed to decrease when they were corroded in recycled water that had been used to oxidize multiple previous samples, suggesting an impact of dissolved corrosion product [20].

3.1.1 (Oxy)hydroxide film adherence

There are three possible outcomes for (oxy)hydroxides formed through corrosion of aluminum in water: (1) retention on the surface as an adherent film, (2) dissolution into the water, and (3) removal in undissolved form (e.g., spallation) [21]. As a result, the amount of oxide on the surface may not directly correlate with the amount of aluminum metal corroded. Experimental studies measuring both have, in fact, observed that the amount of adherent oxide was not sufficient to account for the penetration into the aluminum metal [10, 12, 21].

Aluminum (oxy)hydroxides are known to be soluble in water, and flowing water exacerbates dissolution [3]. Predicted dissolution rates have been used to estimate the metal corrosion rate with good agreement with experimental measurements under certain conditions [21].

Spallation of the oxide film has also been observed under some test conditions, resulting in the loss of larger chunks of oxide and more aggressive localized corrosion following the spallation [12, 13, 18]. Griess et al. [12] observed spallation when the oxide thickness reached approximately 2 mils (50 μm) under simulated reactor conditions, i.e., no irradiation, but with a heat flux through the aluminum sample and exposure to flowing water. However, the onset of spallation after reaching this thickness was unpredictable [12]. Thermal cycling, i.e., stopping and restarting the heat flux through the specimen, produced spallation at lower oxide film thicknesses, as low as about 1 mil (25 μm), which appeared to be triggered by the sudden re-application of the heat flux [12].

High heat fluxes across the oxide cause stress build-up (due to the temperature gradient and resulting thermal expansion variation across the film) which can potentially crack the oxide, contributing to porosity and/or spallation [16]. Pawel et al. [13] reported a strong correlation between the temperature drop across the oxide film and the onset of spallation over a range of pH (4.5–6.0), heat flux (5–20 MW/m^2), and coolant inlet temperature (39–80°C). Specifically, a temperature drop of ≥119°C across the oxide film was strongly associated with spallation [13]. This was attributed to the stresses associated with the oxide growth processes, the temperature gradient, and/or stresses between the film and the underlying metal [13].

3.1.2 Effect of irradiation

Direct, head-to-head comparison of aluminum corrosion under irradiation and under the same conditions without irradiation are sparse. However, a few sources did report comparisons of in-reactor and ex-reactor corrosion.

Dickinson [21] noted that "[c]orrosion rates of active aluminum-clad fuel elements measured in pressurized water reactors or in-reactor test loops have generally been much higher than those measured in isothermal out-of-reactor loops at the same surface temperature, velocity, and water quality," where the corrosion rate corresponded to metal loss. Data for in-reactor corrosion of both dummy elements without heat generation and actual fuel elements were found to agree well if the elements had the same surface temperature, suggesting that the accelerated in-reactor corrosion was not attributed to the influence of having a heat flux through the surface rather than isothermal conditions [21]. The surface temperature was calculated using the Sieder-Tate equation and the bulk water temperature to account for the temperature drop due to the heat flux [21].

By contrast, Breden and Grant [15] compared metal loss for samples located in in-reactor and ex-reactor sections of the same test loop at temperatures from 400–500°F (204–260°C) and found that the corrosion rate increased with increasing distance from the reactor core. The ex-reactor samples featured significantly greater metal loss (by a factor of 3–5) than those in the in-reactor section [15].

Since Refs. [21] and [15] both focused on measurement of metal loss, the impact on the oxide film thicknesses is not clear. However, fitting of a model for oxide growth using both in-reactor data and data from unirradiated test loops with similar ranges of temperature, pH, heat flux, and coolant velocity taken from various sources [16] suggested that in-reactor conditions were "more favorable for oxide growth."

3.1.3 Effect of heat flux

Dickinson [21] reported in-reactor corrosion data from both actual fuel elements (with heat flux) and dummy elements without heat flux, as well as ex-reactor data for electrically heated and unheated samples in the same test loop. For in-reactor elements, both fuel and dummy plates displayed similar corrosion rates [21]. For out-of-reactor tests, heated and unheated samples had similar weights of adherent oxide, but the

heated samples lost about three times as much aluminum metal to the water compared to unheated samples [21]. This ex-reactor data is consistent with Dickinson's model based on the dissolution rate, since the higher surface temperature of heated samples would increase the solubility at the surface and provide a larger driving force for diffusion and dissolution [21].

3.2 Models for aluminum oxidation

Various models have been proposed to predict either the degree of penetration into the original aluminum metal and/or the mass or thickness of adherent oxide as a function of time. Some models are purely empirical fits of experimental data, while others incorporate hypothesized corrosion mechanisms. Due to the complexity of the corrosion process, most of the models are limited to relatively narrow conditions based on experimental data sets used to generate them. This poses particular challenges for predicting oxide thicknesses of ASNF with a complex history of corrosion conditions.

Models of the oxide thickness x_{ox} are frequently power-law models assuming that the growth rate $\mathrm{d}x_{ox}/\mathrm{dt}$ of the oxide film thickness is proportional to the current thickness x_{ox} raised to a power p and with rate constant k (in units of $\mathrm{m}^{p+1}/\mathrm{s}$), i.e.,

$$\frac{dx_{ox}}{dt} = kx^{-p} \tag{1}$$

Assuming constant k and p, the integral form is given by

$$x_{ox}(t) = \left[x_{ox,0}^{p+1} + (p+1)kt\right]^{\frac{1}{p+1}} = \left[x_{ox,0}^{1/n} + \frac{1}{n}kt\right]^{n} \tag{2}$$

where $x_{ox,0} = x_{ox}(t=0)$ is the film thickness at time $t = 0$ (in m) and $n = 1/(p+1)$. A number of studies present correlations in the more specific form

$$x_{ox}(t) = Kt^{n} \tag{3}$$

assuming zero starting thickness $x_{ox,0} = 0$. The rate constants in the two forms are related as $K = (k/n)^{n}$.

Theoretically, the expected exponent can be calculated for certain limiting cases based on the rate-limiting step of the corrosion process. An activation-controlled (i.e., surface-controlled) reaction should yield $n = 1$ or $p = 0$, i.e., a growth rate independent of the film thickness [22]. A reaction limited by diffusion through the oxide film should yield $n = 0.5$ or $p = 1$, i.e., parabolic growth that slows as the film becomes thicker [22], assuming the diffusion coefficient is uniform within the oxide film, as expected for a uniform and isothermal film. In practice, many models empirically fitted power law forms with exponents n between 0.5 and 1, indicating that the oxide growth does slow as the film thickens, although not as rapidly as the theoretical diffusion-controlled case. For example, Pawel et al. [18] fitted Equation (2) with $n = 0.74$, and Griess et al. [12] fitted Equation (3) with $n = 0.76$ or $n = 0.778$.

The rate constant is generally fitted with an Arrhenius-type dependence on temperature. Griess et al. [12] used a rate constant of the form $k = A\exp\left(-4600/T_{x/c}\right)$ where $T_{x/c}$ is the temperature of the oxide-coolant interface and A was set as 443 for pH of 5.0 and 1200 for pH of 5.7–7.0. Pawel et al. [18] used a rate constant (for pH of 5.0) in the form $k = 6.388 \times 10^{7}\exp\left(-9154/\left(T_{x/c} + 1.056q\right)\right]\ \mu\mathrm{m}^{1.351}/\mathrm{h}$, using the heat flux q to modify the effective reaction temperature.

Increasing complexity can be incorporated into the power-law model by using a rate constant and/or exponent that depends on operating conditions in more complex ways. For example, the Kim et al. model [3, 16] is a relatively elaborate power-law model depending on initial oxide thickness, temperature, heat flux, pH, coolant velocity, and an oxide-thickness-dependent thermal conductivity intended to account for

film porosity and cracking. The exponent *p* depended on a temperature and pH-dependent solubility, while the rate constant depended on the oxide-water interface temperature, heat flux, oxide thermal conductivity, current oxide thickness, and coolant velocity. The rate constant also incorporated two constants taking different values for in-reactor versus out-of-reactor conditions, both corresponding to a higher rate constant for in-reactor conditions. This model, with empirically fitted constants, produced good agreement with measurements from their own in-reactor experimental data [3] and for in- and out-of-reactor literature data drawn from various studies by different researchers and under different experimental conditions, but the model had to be solved iteratively [3, 16].

4.0 ASNF cladding service-formed (oxy)hydroxide thicknesses

Data on oxide thicknesses on actual ASNF is sparse and its collection poses substantial challenges. Cladding samples taken from even unfueled portions of the fuel assembly require handling precautions due to contamination, and fueled portions pose even more challenges.

Oxide thickness data available in the literature can be roughly divided into four categories, in increasing order of relevance to assessing the range of oxide thickness on ASNF: 1) Studies unrelated to reactor conditions, such as lab studies to investigate the mechanisms of oxide formation; 2) studies of surrogate cladding samples in (unirradiated) test loops that attempt to replicate certain reactor conditions such as coolant temperatures, flowrate, and/or heat flux through the sample, 3) studies of fueled or unfueled samples tested in an actual reactor, and 4) characterization of actual ASNF discharged from a reactor. Since the full set of conditions controlling oxide thickness is not well understood and, in particular, there is evidence for significant differences between in-reactor and out-of-reactor oxide growth for unclear reasons, results from out-of-reactor surrogate studies should be used with caution, and the present report focuses on in-reactor data.

4.1 Prefilmed ASNF

Prefilming of fuel is a process intended to form a protective layer of oxide prior to use in a reactor in order to reduce the amount of corrosion and oxide growth during reactor operation.

4.1.1 Advanced Test Reactor (ATR)

Advanced Test Reactor (ATR) fuel is prefilmed to form a boehmite layer prior to irradiation. The prefilming process has changed over the lifetime of the reactor. Until 1994, fuel elements were exposed to flowing demineralized water at 340°F ± 10°F (171°C ± 6°C) in the Hydraulic Test Facility (HTF) prior to loading in the reactor, which formed the boehmite film [23]. Later, the prefilming was performed by immersion in deionized water at 185°C for 18 hours in an autoclave [22, 24]. Boehmite prefilms resulting from the autoclave approach were characterized and determined to be equivalent to prefilms generated using the HTF [22]. This well-crystallized boehmite film (typically 3 μm thick, although thicknesses in the range 2–6 μm have been measured [24]) is expected to protect against further corrosion during reactor service and post-discharge storage. To further inhibit corrosion, the ATR maintains a nominal pH of 5.0 [11].

Griebenow [25] reported oxide measurements obtained during post-irradiation destructive examination of ATR fuel elements operated during two phases of the ATR startup program. The fuel was operated at power for either 35 or 27 days depending on the fuel element and was stored underwater in the ATR canal for >6 months prior to examination. Oxide thicknesses on the convex surfaces of many fuel plates were measured using the eddy current technique. Reported per-plate maximum oxide thicknesses ranged from 0.49–1.75 mils (12–44 μm) for different plates [25]. Metallographic characterization found thicknesses consistent with the eddy current technique, and indicated that thicknesses on the convex and concave surfaces were comparable [25]. The convex surface of plate 19, which is exposed to the outside coolant channel and is the most accessible plate surface without disassembly, tended to have lower oxide loading than the surfaces facing inner water channels [25].

Full sets of oxide thickness measurements (not just the maximum) were plotted for a few fuel plates. Sixteen measurements from (interior) fuel plate 5 from an element operated for 35 days and stored wet for >6 months were plotted as a function of the initial fuel plate surface temperature (~120–240°F / ~49–116°C), showing measured oxide thicknesses ranging from ~0.1–1.5 mil (3–39 μm) with the majority of measurements in the upper end of the range [25]. The average of the measured values is ~1 mil (25 μm) (note that the spacing of the measurements is unspecified), and 10 of 16 data points measured >1 mil (25 μm). The measured oxide thicknesses generally increased non-linearly with increasing surface temperature. Two data points at relatively high temperature fell significantly below the curve and were noted to possibly reflect spalling of oxide [25].

The oxides measured from the stored elements significantly exceeded thicknesses predicted by the Griess correlation [12] and displayed a two-layer structure under metallographic examination, leading to speculation that additional oxide growth may have occurred during the >6 months wet storage. Therefore, underwater oxide thickness measurements were performed on the outer surface of plate 19 (accessible without disassembly) for two freshly discharged fuel elements, with results shown in Figure 4-1. The measured oxide thicknesses ranged from ~0.03–0.7 mils (0.6–18 μm), with the lowest thickness at the top of the plate. The oxide thickness ramped up over the first ~10 in of the plates and then reached roughly uniform thickness in the range ~0.5–0.7 mils (~13–18 μm) over the majority of the plate [25]. The average of all measured thicknesses (including the end region with thinner oxide) was 0.62 mils (13 μm, from 9 measurements) for one plate and 0.46 mils (12 μm, from 6 measurements) for the other.

The maximum oxide thicknesses for the freshly-discharged plates (0.7 and 0.6 mils) were comparable to the plate-19 maximum oxide thicknesses reported for the >6-month-stored fuel elements (0.49, 0.51, 0.72, and 1.32 mils), and the earlier destructive evaluation showed that the plate 19 outer surface tended to have lower oxide loading than interior plates [25]. Therefore, there is no strong evidence that the oxide loading on the freshly discharged fuel elements was significantly lower than that measured after wet storage.

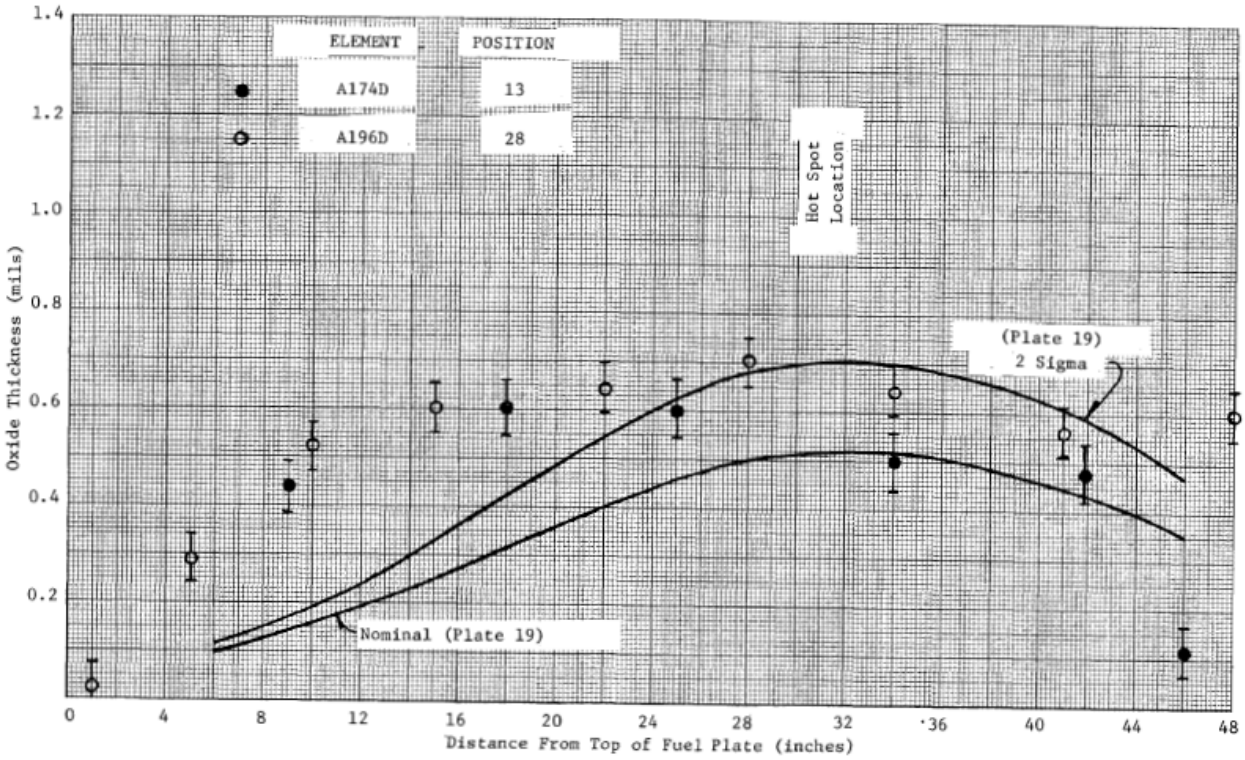

Figure 4-1. ATR Cycle 4B oxide measurements, taken from convex surface of plate 19 for two different fuel elements; solid lines correspond to predictions of an ORNL correlation [25].

Vinjamuri [26] reported post-irradiation examination of two failed ATR fuel elements with pinhole corrosion defects. The failures were detected during the reactor cycle due to fission products leaking into the coolant, and the failed elements were examined after the end of the cycle, first in the storage canal to identify the failed elements and then in the hot cells. The investigation focused strictly on the defects, which occurred at approximately the maximum flux region (74 cm from the top of the plate and near the edges), and on the defects' immediate surroundings; this included taking metallographic samples to inspect the cross-section near the pinhole defects. Oxide thicknesses of 23 μm on the convex surface of one plate (plate 13 in its fuel element) and 25 and 28 μm on the outer and inner cladding surfaces of the other (plate 9) were reported [26]. Since this characterization was performed only in the immediate vicinity of the cladding failures, it is not known how the thickness in the defect region compares to the remainder of the fuel element surfaces. However, the oxide thicknesses measured here, for interior plates, are well within the range measured by the more extensive survey in Ref. [25] and are close to the average of the plate 5 measurements from that study.

As part of current ASNF dry storage research, characterization of oxide on ATR fuel plates was performed by cutting small samples from side plate material attached to the end boxes and from the corners of fuel plates without breaching the fuel meat, and by taking scrapings from the surface of dry-stored ATR plates [24, 27]. The investigation aimed to identify both thickness and type of oxide.

The wet-stored samples came from ATR end boxes, which are unfueled structures cut from the ATR spent fuel assemblies prior to moving the assemblies to dry storage. The location of the cut leaves a small portion of the fuel assembly side plate attached to the end box, and the side plate region was the target of the sampling. The history of individual end boxes was not tracked, so the samples' specific irradiation and storage histories are unknown [24]. The three dry-stored SNF elements were removed from the reactor in 1985, stored wet until 1997, and then moved to dry storage. Samples were taken from plate 19 of each fuel

element, with two samples of scraped oxide per element (6 total) taken from the convex surface, along with cut samples from all four corners of each plate (12 total) outside of the fuel meat [27].

Cross-sectional SEM/EDS of the corner samples showed oxide thickness in the range of about 1–4 μm on the wet-stored ATR samples [24] and 2–6 μm on dry-stored samples [27], equivalent to the expected thicknesses of the initial prefilm. During handling of wet-stored ATR materials for sampling, localized puffy oxide deposits were observed on some elements at exposed edges [24, 27]. This was believed to be the result of damage to the protective boehmite layer from abrasion against the fuel racks, use of friction tools and/or removal of the endboxes, which exposed fresh aluminum surface to the water and enabled further corrosion [24, 27].

XRD of wet-stored pieces was inconclusive, although energy-dispersive X-ray spectroscopy (EDS) confirmed the presence of an oxide that could not be more specifically identified [24]. Thermogravimetric analysis (TGA) of the cuttings up to 300°C observed negligible mass loss [24], showing no evidence of significant trihydroxide content, since aluminum trihydroxides (but not boehmite) are expected to start thermally decomposing at <300°C [28, 29]. XRD of sample material scraped from the surface of dry-stored ATR fuel, capturing both oxide and some underlying aluminum, identified the oxide as predominately boehmite [27]. TGA of the scraped material using a step-wise temperature increase from 100°C to 500°C, with 1-hour holds at every 100°C increment, observed as much as 7% mass loss, with the most significant losses occurring in the 200–300°C range and lower losses between 300 and 500°C [27].

4.1.2 Other prefilmed ASNF

Kim et al. [3] reported systematic oxide thickness measurements for small (101.6 x 25.4 x 1.4 mm), fueled test plates tested in the ATR during RERTR-6 and RERTR-7A tests. The plates were prefilmed for 4 hours at 185°C and 1 MPa to produce an oxide layer of about 1 μm (the same temperature as standard ATR prefilming, but shorter duration). Each test included 32 test plates total, not all of which were included in the oxide thickness measurements reported. The heat flux, total irradiation time, and coolant flowrates differed between the two tests, but the combination of heat fluxes and flowrates maintained similar oxide-water interface temperatures. The pH was maintained in the range 5.1–5.3 for both tests. The test plates were in the reactor for multiple cycles (3 cycles totaling 135 days for RERTR-6 and 2 cycles/90 days for RERTR-7A). Oxide thicknesses were measured by the eddy current technique at nine locations spaced over the fuel meat in a 3x3 grid on both sides of the plate for a total of 18 measurements per plate.

For RERTR-6, oxide thickness measurements were reported for 26 plates, with an overall range of 0.4–13.4 μm and mean of 3.9 μm. For 24 plates from RERTR-7A, the overall mean thickness was almost identical, 4.1 μm, but with wider variation for an overall range of 0.2–21.3 μm. Per-plate average thicknesses (average of 18 measurements) ranged from 2.0–6.3 μm for RERTR-6 and 1.2–9.7 μm for RERTR-7A [3]. For RERTR-7A, the oxide thickness along one side of the plate (locations denoted as A, D, and G, both front and back) averaged approximately double that of the other six positions; for RERTR-6, the same locations averaged slightly higher than the rest of the plate. This may be attributable to the plate positioning "sideways to the reactor core so that one side of the plate width had a higher power than the other side" [3]. The authors noted that the oxide thicknesses measured from RERTR-6 and RERTR-7A were substantially lower than those reported in the literature for other reactors, which they attributed to a combination of the prefilming and the low pH (5.1–5.3) of the ATR coolant [3].

Some early HFIR cores were pretreated in boiling water for 24 hours to produce a prefilm [30]. Unlike the high-temperature (185°C) autoclave prefilming used for ATR, the oxide generated by this pretreatment was determined to be unprotective, resulting in the growth of thicker oxide films and higher temperature drops during reactor operation than the use of non-pretreated HFIR fuel, and the prefilming was discontinued [30]. The HFIR coolant is maintained at a pH of 5.0, with inlet and outlet temperature ranges of 110–120°F (43–49°C) and 150–160°F (66–71°C), respectively, and a speed of about 55 ft/s (17 m/s) through the fuel [30].

The fuel has a useful lifetime of about 23 days (2300 MWd), and the average heat flux is calculated to be 0.8×10^6 Btu/h·ft^2 (2.5 MW/m^2) [30].

Richt et al. [30] characterized HFIR fuel cooled for ~1 year in wet storage before examination to ensure fuel temperature would not exceed ~300°F (~150°C) during handling in the hot cells. Oxide thicknesses were assessed on three plates of a pretreated outer HFIR assembly (designated 5-O) by measuring the fuel plate thickness at numerous locations before and after chemical stripping of the oxide and by metallographic measurements (at fewer locations) on the fourth, cross-sectioned plate [30]. The oxide thicknesses on the pretreated assembly were in the range ~0.2–1.6 mils (~5–41 μm), averaging about 0.8 mil (21 μm). XRD identified scrapings of the oxide as bayerite, and spallation had occurred in regions predicted to be the hottest.

The prefilmed inner fuel assembly (designated 5-I) irradiated with outer assembly 5-O had soft, white bayerite deposits blocking the bottom end of some coolant channels; however, no characterization of individual fuel plates or oxide thickness measurements was performed for assembly 5-I [30]. The authors assumed the bayerite deposits blocking the channels on 5-I formed during the ~1 year wet storage, since high coolant flow rates would likely have dislodged them during reactor operation [30].

4.2 Non-prefilmed ASNF

Richt et al. [30] also conducted post-irradiation characterization of one inner (49-I) and one outer (21-O) non-prefilmed HFIR fuel assembly, including the destructive evaluation of four fuel plates per assembly as described above. The metallographic measurements were found to have fairly good agreement with the values obtained from the plate thickness [30]. Thickness profiles showing both sets of measurements are shown in Figure 4-2. Measurements were spaced axially at 1-in intervals for the length of the plate and at 3 locations across the width of the fuel plate: near the inner edge, outer edge, and at the point of thickest fuel core.

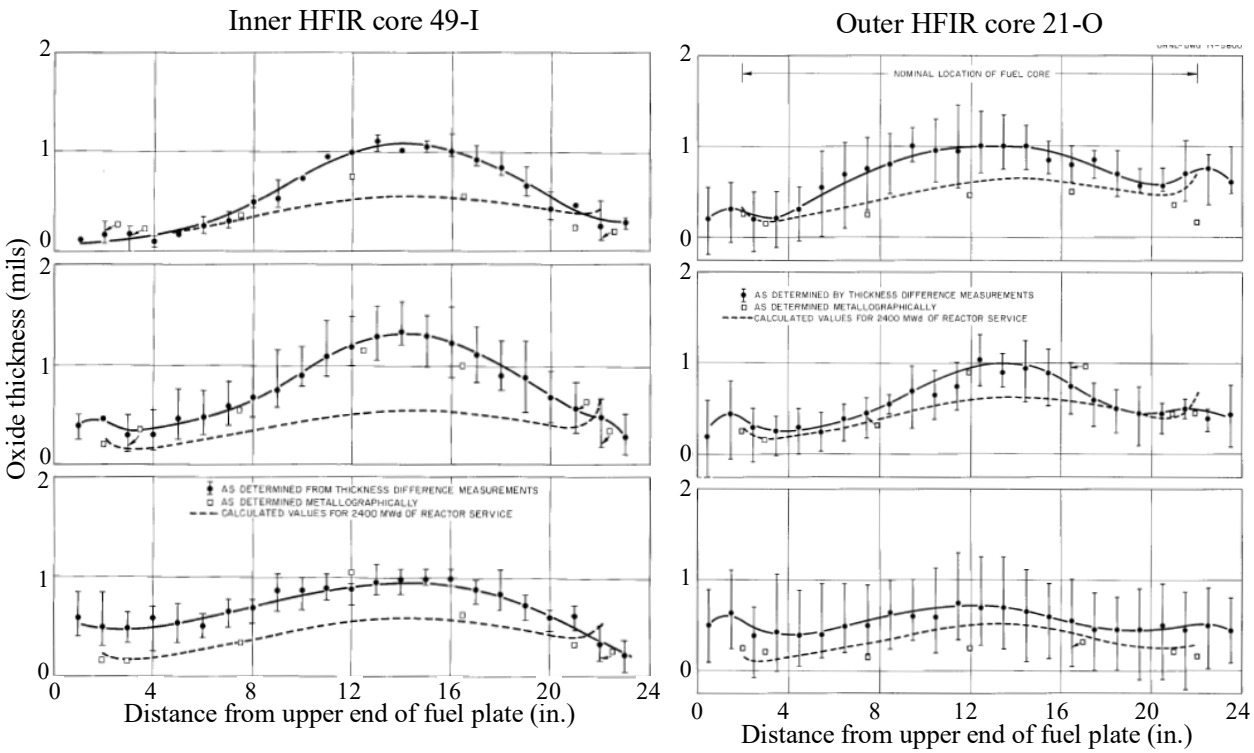

Figure 4-2. Axial film thickness profiles on fuel plates from HFIR inner fuel element 49-I (left) and outer fuel element 21-O (right) along three lines: near inner edge of plate (top), over fuel meat "hump" (middle), and near outer edge of plate (bottom). Filled markers obtained by thickness-difference measurements before and after oxide removal; unfilled markers from metallography [30].

The measured oxide thicknesses were found to consistently exceed the values predicted based on the Griess correlation [30]. The oxide showed no signs of spallation and was thickest near the middle of the plate axially. The range of oxide thicknesses measured from fuel plate thickness was ~0.2–1.1 mils (5–27 μm), averaging ~0.6 mils (~15 μm), for the outer assembly 21-O and ~0.1–1.3 mils (3–33 μm), averaging ~0.7 mils (17 μm), for the inner assembly 49-I. Cross-section images indicated two distinct layers of oxide of approximately equal thickness, and XRD of scraped oxide identified predominantly bayerite on the outer assembly plates and a roughly 50%-50% mixture of bayerite and boehmite on the inner assembly plates [30].

Mieleszczenko et al. [31] reported results of post-irradiation examination of fuel irradiated in the MARIA Reactor in Poland. The average coolant speed ranged from 5.1–9.2 m/s; other coolant properties and temperatures were not specified. The elements MC001 and MC002 were irradiated to burnups of ~5900 MWh and 4025 MWh, respectively. Eddy current measurements of adherent oxide thickness (Figure 4-3) ranged from near zero at the top of the assembly to maximum values of slightly over 30 μm and just under 40 μm for the two SNF assemblies tested. The average of the evenly spaced eddy current measurements (every 100 mm from 0 to 900 mm) was about 19 μm for element MC001 and 12 μm for MC002. XRD of oxide samples found predominantly $Al(OH)_3$ with a small amount of boehmite [31]. Visual inspection of MC001 showed "separation of the oxide layer" in high-temperature regions, and samples detached from this element were reported to measure approximately 30–50 μm thick [31]. Unfortunately, very little information about the methods of obtaining and measuring these samples was provided.

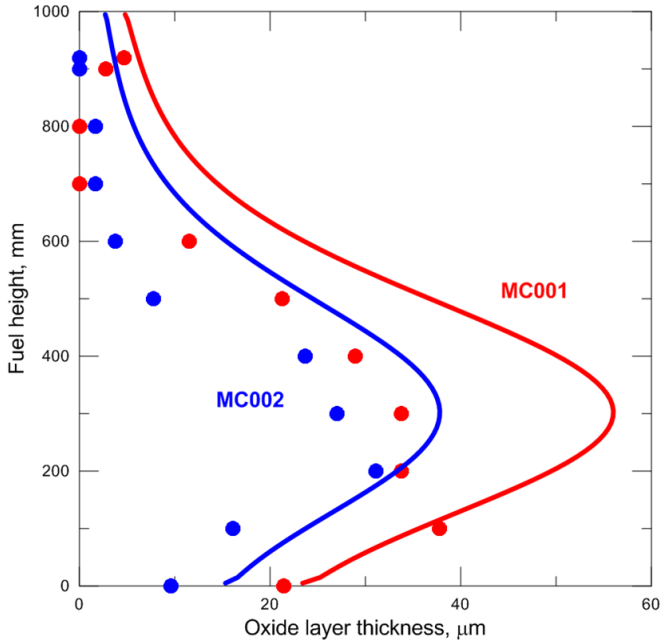

Figure 4-3. Oxide thickness measurements along an axial profile, measured by eddy current; solid lines correspond to theoretical predictions [31].

Sears et al. [32] reported post-irradiation examination for three prototype aluminum-clad, Al-64 wt.% U_3Si_2 fuel elements tested in the Canadian heavy-water-cooled NRU reactor. The reactor coolant had nominally 5.5–6.5 pH, 37°C inlet temperature, 70°C outlet temperature, and 8.8 m/s velocity, and the maximum fuel rod power was 2.1 MW [32]. The prototype fuel rods occupied several different positions over the course of their full irradiation, in line with typical operation of the reactor, and were stored for ~1 year in a light-water fuel pool during reactor shutdown (pH 7.6–7.7) [32].

Underwater visual inspection showed a light-colored oxide over the fueled section of the cladding and a darker oxide over the unfueled ends [32]. Oxide thicknesses were obtained from three metallographic samples per element, taken from the top, middle, and bottom, showing an overall range of 15–80 μm for the nine total samples [32]. These thicknesses were higher than expected compared to previous NRU high-burnup fuel rods reported to typically have 20–40 μm thick oxides [32]. The authors speculated that the unusual thickness might be attributable to the ~1 year of storage in a light-water pool during a reactor shutdown, since the pH and impurity levels in the pool water were known to be higher than that of the reactor heavy-water coolant [32] (the operating pH range of this reactor was also higher than that used for ATR and HFIR). For two of the three fuel elements, the maximum oxide thickness (including the 80 μm overall maximum) was observed on the middle sample axially; for the third element, the maximum oxide thickness was observed at the top of the rod. No characterization of the oxide type was reported.

Kim et al. [3] briefly summarized reported oxide thicknesses (generally a single value with specified uncertainty for each source) for multiple studies as part of developing and validating an oxide growth model. The reported values, in order of increasing oxide thickness, are given in Table 4-1 along with the irradiation conditions specified. None of the operating conditions obviously dominates the determination of oxide thickness. The lowest oxide thickness (for ORR A101) had the lowest pH range of the reported specimens, and the highest oxide thickness (UMUS MEU) was one of several at the highest pH of 6.5. However, the oxide thicknesses of tests at pH of 6.5 were scattered across the entire range of reported thickness values, and neither ORR A101 nor UMUS MEU were at the extreme ends of the range for any other operating condition.

Table 4-1. Oxide thickness reported by Kim et al. [3]

Name	Oxide thickness	Duration (days)	pH	Oxide-water interface temperature	Heat flux (MW/m^2)	Coolant velocity (m/s)
ORR A101	14 ± 2 µm	~150	5.5–6.3	~95–80°C (decreasing in stages)	~1.9–1.6 (decreasing in stages)	8.5
UMUS LEU 90 mm	16 ± 5 µm	~48	6.5	82.6°C	1.7	8.3
FUTURE (right plate)	21 ± 3 µm	40	5.9 to 6.2 (increasing linearly)	122 to 109°C (decreasing linearly)	3.2 to 2.7 (decreasing linearly)	12
FUTURE (left plate)	27 ± 4 µm	40	5.9 to 6.2	128 to 116°C	3.4 to 2.9 MW/m^2	12
SIMONE LC-04	43 ± 7 µm	~500	6.5	~52–75°C (varying non-monotonically)	~0.35–0.85 (varying non-monotonically)	6.6
UMUS MEU 274 mm	61 ± 7 µm	~48	6.5	107.4°C	2.5 MW/m^2	8.3

Oxides on unfueled portions of several ASNF materials removed from storage at the Savannah River Site (SRS) were characterized as part of the current ASNF dry storage investigation [17, 33]. These included a sample from the end of a Materials Test Reactor fuel plate from the RU-1 reactor in Uruguay that had been stored dry since coming out of the reactor [33] and two samples from wet storage: an end cropping from a Missouri University Research Reactor (MURR) fuel assembly and an unfueled region of a Mark-16B fuel assembly from an SRS production reactor [17].

The RU-1 fuel element was operated in the reactor for approximately 8 years, 5.75 years under power, and was stored dry for ~31 years (11 years in Uruguay and 20 years at SRS). The cladding was estimated to be around 70°C during irradiation, but the pH and coolant flow rate are unknown [33]. Exact histories for the MURR and Mark-16B are not available, but general information is available based on the reactor operation. The MURR would have operated in-reactor for a total of 126–133 days, in cycles of 6.3 days in-reactor alternating with at least 7 days in wet storage. MURR inlet and outlet coolant temperatures were 60 and 71°C, respectively, and its wet storage pool had a mixed bulk temperature of 38°C. The pool pH averaged 5.8. The Mark-16B cropping came from the top (inlet end) of an assembly irradiated in an SRS heavy-water reactor, so it would have experienced coolant temperatures close to 38°C and ~7 months of reactor operation [17]. The SRS wet storage pool, where the MURR and Mark-16B croppings were stored for <18 years (MURR) and ~40 years (Mark-16B) had average pH 6.5 and average temperature of 22°C.

Cross-sectional SEM was performed on a single sample for each material (all taken from unfueled end regions of their fuel elements). Oxide thicknesses in the ranges 5–10 µm for the MURR and 5–15 µm for the Mark-16B samples were observed [17]. The oxide on the dry-stored RU-1 sample appeared thin (~0.2

μm) or indiscernible on most of its surface, interspersed with occasional patches measuring ~5–25 μm thick [33].

X-ray diffraction (XRD) indicated the presence of trihydroxides ($Al(OH)_3$, bayerite or gibbsite) on all of these samples. A mixture of bayerite and boehmite was identified on the MURR and a mixture of bayerite, boehmite, and gibbsite on the Mark-16B [17]. The relative size of the XRD peaks suggested that the fraction of boehmite relative to trihydroxides (bayerite and gibbsite) was lower on the Mark-16B that is believed to have operated at lower temperature. XRD of the dry-stored RU-1 sample detected small gibbsite peaks as well as a small peak tentatively attributed to boehmite [33].

5.0 Conclusions

Oxide thickness measurements on post-irradiation ASNF are sparse in the literature, and reported values have covered a wide range, ranging from <1 μm to as high as 80 μm. This data includes single-point maximums (rather than fuel surface average) and oxides formed under conditions including high pH. The type of oxide was not reported in many studies. Bayerite or mixed trihydroxide-boehmite layers were found on several fuels (HFIR, MARIA, MURR, Mark-16B, RU-1), while boehmite was reported by one study of ATR.

For studies that reported systematic measurements from numerous points on a plate (rather than only maximums or isolated values), the averages of the sets of oxide thickness measurements (representing measurements from 8 fuel elements from 3 reactors) ranged from 12 to 25 μm. The per-plate average oxide thicknesses for RERTR-6 and RERTR-7A test plates in the ATR, 1.2–9.7 μm [3], were significantly lower than the per-plate averages reported by Ref. [25] for ATR fuel itself, despite the test plates being exposed through several reactor cycles.

Axial oxide thickness profiles tended to peak near the middle of fuel plates [25, 30, 31] with lower thicknesses near the plate ends. This is presumably associated with higher cladding temperatures over the fuel meat. RERTR samples measurements support this hypothesis given that the oxide was thickest on average along one *side* of the fuel meat when the plates were deliberately oriented to produce higher power on one side. Unfortunately, this suggests that oxide measurements from small and/or unfueled samples and/or from unfueled portions of ASNF (which typically occur around the edges of the fuel plates) are likely to underestimate the average oxide loading. ATR measurements [25] indicated that even measurements over the fuel meat may underestimate oxide loadings for the full assembly if taken only from an external fuel plate.

This literature survey indicates that average oxide thicknesses of 12–25 μm are reasonable to expect on ASNF plates, including on elements from the Advanced Test Reactor and High Flux Isotope Reactor, with localized maximums reaching higher values. The spread of available data and the variety of prefilm, reactor service, and post-discharge storage conditions does not enable identification of a bounding oxide thickness, and average oxide thicknesses exceeding 25 μm for ASNF may occur.

6.0 References

[1] E. Eidelpes, J. Jarrell, T. E. Lister, G. P. Horne, E. H. Parker-Quaife, J. K. Conrad, C. D. Pilgrim, A. W. Abboud, P. L. Winston, R. E. Smith, A. L. d'Entremont, B. C. Randall, R. Sindelar. Technical Basis for Extended Dry Storage of Aluminum-clad Spent Nuclear Fuel. *Journal of Nuclear Materials* 577, 154299, https://doi.org/10.1016/j.jnucmat.2023.154299, 2023.

[2] ASTM C1553-21. Standard Guide for Drying Behavior of Spent Nuclear Fuel. 2021.

[3] Y. S. Kim, G. L. Hofman, A. B. Robinson, J. L. Snelgrove, N. Hanan. Oxidation of aluminum alloy cladding for research and test reactor fuel. *Journal of Nuclear Materials*, 378(2):220–228, 2008.

[4] K. Wefers and C. Misra. Oxides and hydroxides of aluminum. Technical Report Alcoa Technical Paper #19, Alcoa Laboratories Pittsburgh, PA, 1987.

[5] W. J. Bernard and J. J. Randall. An investigation of the reaction between aluminum and water. *Journal of The Electrochemical Society*, 107(6):483–487, 1960.

[6] B. R. Baker and R. M. Pearson. Water content of pseudoboehmite: a new model for its structure. *Journal of Catalysis*, 33(2):265–278, 1974.

[7] W. Vedder and D. A. Vermilyea. Aluminum+ water reaction. *Transactions of the Faraday society*, 65:561–584, 1969.

[8] Robert S. Alwitt. The anodic oxidation of aluminum in the presence of a hydrated oxide. *Journal of The Electrochemical Society*, 114(8):843–848, 1967.

[9] R. Demichelis, B. Civalleri, Y. Noel, A. Meyer, and R. Dovesi. Structure and stability of aluminium trihydroxides bayerite and gibbsite: A quantum mechanical ab initio study with the crystal06 code. *Chemical Physics Letters*, 465(4-6):220–225, 2008.

[10] R. L. Dillon. Dissolution of aluminium oxide as a regulating factor in aqueous aluminum corrosion. Technical Report HW-61089, General Electric Co., Richland, WA (USA). Hanford Atomic Products Operation, 1959.

[11] E. Shaber and G. Hofman. Corrosion Minimization For Research Reactor Fuel. Technical Report INL/EXT-05-00256, Idaho National Laboratory, 2005.

[12] J. C. Griess, H. C. Savage, J. L. English. Effect of heat flux on the corrosion of aluminum by water. Part IV. Tests relative to the advanced test reactor and correlation with previous results. Technical report ORNL-3541, Oak Ridge National Laboratory, 1964.

[13] R. E. Pawel, G. L. Yoder, C. D. West, and B. H. Montgomery. The development of a preliminary correlation of data on oxide growth on 6061 aluminum under ANS thermal-hydraulic conditions. Technical Report ORNL/TM-11517, Oak Ridge National Laboratory, 1990.

[14] R. E. Pawel, G. L. Yoder, D. K. Felde, B. H. Montgomery, M. T. McFee. The Corrosion of 6061 Aluminum Under Heat Transfer Conditions in the ANS Corrosion Test Loop. *Oxidation of Metals* 36, pp. 175-194, 1991.

[15] C. R. Breden and N. R. Grant. Summary of corrosion investigations on high-temperature aluminum alloys. period covered: February 1955-October 1956. Technical report ANL-5546, Argonne National Laboratory, 1960.

[16] Y. S. Kim, G. L. Hofman, N. A. Hanan, J. L. Snelgrove. Prediction model for oxide thickness on aluminum alloy cladding during irradiation. In *2003 International Meeting on Reduced Enrichment for Research and Test Reactors*, Chicago, 2003.

[17] L. C. Olson, C. Verst, A. L. d'Entremont, R. E. Fuentes, and R. L. Sindelar. Characterization of oxide films on aluminum materials following reactor exposure and wet-storage in the SRS L-Basin. Technical Report SRNL-STI-2019-00058, Savannah River National Laboratory, 2019.

[18] S. J. Pawel, D. K. Felde, and R. E. Pawel. Influence of coolant pH on corrosion of 6061 aluminum under reactor heat transfer conditions. Technical report, Oak Ridge National Laboratory, 1995.

[19] Robert S. Alwitt. The growth of hydrous oxide films on aluminum. *Journal of The Electrochemical Society*, 121(10):1322–1328, 1974.

[20] D. G. Altenpohl. Use of boehmite films for corrosion protection of aluminum. *Corrosion*, 18(4):143t–153t, 1962.

[21] D. R. Dickinson. Oxide dissolution in corrosion of aluminum cladding on nuclear reactor fuel elements. *Corrosion*, 21(1):19–27, 1965.

[22] E. L. Shaber and P. A. Lessing. Boehmite coating evaluation. Technical Report TRA-ATR-1123, Lockheed Idaho Technologies Company, 1996.

[23] W. D. Richins and G. K. Miller. Analysis of the ATR fuel element swaging process. INEL-95/0558, Idaho National Engineering Laboratory, 1995.

[24] P. Winston, C. Adkins, J. Aguiar, B. Hernandez, D. Murray, K. Tolman, A. Winston. Aluminum Spent Fuel Performance in Dry Storage Task 4 Objective 1 Initial Characterization of ATR End Box Samples. Technical Report INL/EXT-18-51230, Idaho National Laboratory, 2018.

[25] M. L. Griebenow. ATR Extended Burnup Program. doi:10.2172/4717775, Aerojet Nuclear Company, 1971.

[26] K. Vinjamuri. Postirradiation Examination of Advanced Test Reactor Fuel Elements XA377N and XA379N. Technical Report EGG-TFBP-5968, Idaho National Engineering Laboratory, 1982.

[27] P. Winston, S. Middlemas, A. Winston, J. Aguiar, X. Liu, K. Tolman. Aluminum Spent Fuel Performance in Dry Storage Task 4 Aluminum Oxide Sampling of ATR Dry-Stored Fuel. Technical Report INL/EXT-20-58404, Idaho National Laboratory, 2020.

[28] J. W. Newsome, H. W. Heiser, A. S. Russell, H. C. Stumpf, ALUMINA PROPERTIES. Technical Paper No. 10, Second Revision. Aluminum Co. of America. Alcoa Research Labs., New Kensington, Penna., 1960.

[29] A. L. d'Entremont, R. E. Fuentes, M. G. Shalloo, T. W. Knight, R. L. Sindelar, Thermal Dehydration of Aluminum (Oxy)hydroxides on Fuel Cladding Material. Waste Management Symposia 2020, #20200, 2020.

[30] A. E. Richt, R. W. Knight, G. M. Adamson, Jr. Postirradiation Examination and Evaluation of the Performance of HFIR Fuel Elements. Technical Report ORNL-4714, Oak Ridge National Laboratory,1971.

[31] W. Mieleszczenko et al.. Summary of Works Over MARIA Reactor Core Conversion From HEU to LEU Fuel. *RERTR 2012 — 34th International Meeting On Reduced Enrichment For Research And Test Reactors*, 2012.

[32] D.F. Sears, M. F. Primeau, C. Buchanan, and D. Rose. Post-irradiation examination of prototype Al-64 wt% U3Si2 fuel rods from NRU. *Proceedings of the 1994 International Meeting on Reduced Enrichment for Research and Test Reactors*, Technical Report ANL-RERTR-TM-20, p. 124, 1994.

[33] L. C. Olson, R. E. Fuentes, A. L. d'Entremont, and R. L. Sindelar. Characterization of oxyhydroxides on a dry-stored fuel plate from L-Basin. Technical Report SRNL-STI-2018-00428, Savannah River National Laboratory, 2018.

Distribution:

SRNL:
Records Administration (EDWS)
william.bates@srnl.doe.gov
Boyd.Wiedenman@srnl.doe.gov
frank.pennebaker@srnl.doe.gov

INL:
josh.jarrell@inl.gov
Elmar.Eidelpes@inl.gov